Draft version November 17, 2008
Preprint typeset using LaTeX style emulateapj v. 10/09/06

BALMER EMISSION LINE PROFILES AND THE COMPLEX PROPERTIES OF BROAD LINE REGIONS IN ACTIVE GALACTIC NUCLEI

G. La Mura[1], F. Di Mille[1], S. Ciroi[1], L. Č. Popović[2,3], and P. Rafanelli[1]

Draft version November 17, 2008

ABSTRACT

In this work we analyze a sample of AGN spectra, selected from the 6$^{\rm th}$ Data Release of the Sloan Digital Sky Survey, exploiting a generalized technique of line profile analysis, designed to take into account the whole profiles of their broad emission lines. We find that the line profile broadening functions result from a complex structure, but we may be able to infer some constraints about the role of the geometrical factor, thus improving our ability to estimate AGN properties and their relation with the host galaxy. Our results suggest that flattening and inclination within the structure of the Broad Line Region (BLR) must be taken into account. We detect low inclinations of the BLR motion plane with respect to our line of sight, typically $i \leq 20°$, with a geometrical effect which generally decreases as the line profile becomes broader.

Subject headings: galaxies: active — galaxies: nuclei — galaxies: Seyfert — line: profiles — quasars: emission lines

1. INTRODUCTION

During the past decades, spectroscopic observations provided a fundamental starting point for our understanding of the physical processes in Active Galactic Nuclei (AGN). In particular, the study of broad emission lines, characterizing the spectra of many objects at different wavelengths, is a key feature to penetrate their intrinsic properties (Osterbrock 1989). Unfortunately, a correct interpretation of the observations requires to collect information in various spectral ranges and for long monitoring times, a task which is currently possible only in a fairly small number of cases. While much work has been devoted to calibrate empirical methods which should be able to deal with larger samples (see e. g. Kaspi et al. 2000, 2005; Bentz et al. 2006), the fundamentally unknown structure in the core of AGN influences the physical interpretation of spectra with a geometrical factor, whose value depends on the structure and orientation of the source (see for instance Vestergaard et al. 2000; Nikołajuk et al. 2005; Marziani et al. 2006; Decarli et al. 2008a).

The prominent broad emission lines, visible in the spectra of many AGN, originate close to the central power source, in the so called Broad Line Region (BLR). Because of its small distance from the power source, the BLR is in strong interaction with the radiation field produced by the central engine and with its gravitational forces. Many interesting details about the physics of processes that are taking place within AGN can be identified in the signal of the BLR, but they suffer from a still missing complete picture of the complex kinematical and thermodynamical properties of the line emitting plasma. Since it is not yet possible to directly observe the spatial distribution of the broad line emitting medium, although many important achievements were obtained in the angular resolution of AGN cores at radio wavelengths (e. g. Kellerman et al. 1998, and references therein), spectroscopic data are still the most useful way to investigate physics within the BLR. The well known Reverberation Mapping (RM) technique (see Blandford & McKee 1982), based on multiple spectroscopic observations, provides a reliable way to constrain the volume where the nuclear activity is confined and, thus, to estimate the mass concentration therein (e. g. Wandel 1999; Peterson & Wandel 2000; Peterson et al. 2004).

The most commonly accepted interpretation of AGN puts a Super Massive Black Hole (SMBH) in the role of the central engine, since matter accretion into its gravitational field provides the required power to account for many observational properties. Once the size of the BLR is known, it is possible to estimate the mass of the SMBH:

$$M_{BH} = f \cdot \frac{R_{BLR} \Delta v^2}{G}, \qquad (1)$$

where G is the gravitational constant, f represents the geometrical factor which accounts for the unknown distribution of the line emitting material, R_{BLR} is a characteristic BLR radius, and Δv is an estimate to the velocity field, usually coming from the width of the emission lines. In their recent work, Kaspi et al. (2005) found that a power law relationship of the form $R_{BLR} \propto (5100\,\text{Å}\, L_{5100})^{\alpha}$ may adequately describe AGN, although the actual value of the power law exponent and the luminosity range, where the relationship holds in different AGN classes, still have to be constrained (Kaspi et al. 2007; Kelly et al. 2007; Laor 2007; McGill et al. 2008). Bentz et al. (2006) argued that, at least for moderate luminosity sources, with $L_{bol} \leq 10^{46}\,\text{erg}\,\text{s}^{-1}$, it is likely that $\alpha \simeq 0.52$, not far from the predictions of simple photoionization calculations giving $\alpha \sim 0.5$.

Unfortunately, the problems introduced by our limited knowledge about the actual structure of the BLR badly affect the value of such estimates, rising many uncertainties which make it quite difficult to infer the physical

[1] Department of Astronomy, University of Padova, Vicolo dell'Osservatorio, I-35122 Padova, Italy; giovanni.lamura@unipd.it, stefano.ciroi@unipd.it, francesco.dimille@unipd.it, piero.rafanelli@unipd.it.
[2] Astronomical Observatory, Volgina 7, 11060 Belgrade, Serbia; lpopovic@aob.bg.ac.yu.
[3] Isaac Newton Institute of Chile, Yugoslavia Branch, 11060 Belgrade, Serbia.

properties of AGN or to study their relation with the host galaxy environment. During the past years, a lot of work has been devoted to understand the relationship between the BLR dynamics and the corresponding broad emission line profiles (e. g. Capriotti et al. 1980, 1981; Ferland et al. 1992; Peterson & Wandel 1999; Korista & Goad 2004), but, while the former is probably very complex, often with evidence for multiple components (Popović et al. 2004), the latter is the result of a combination of effects involving the gas motion pattern and the radiation transfer across an environment which is only approximately understood.

In this paper we describe the results we obtained by analyzing the kinematical properties of the BLR gas in a sample of AGN extracted from the Sloan Digital Sky Survey (SDSS) database, by means of a technique exploiting the cross-correlation method and the Gauss-Hermite profile fitting to infer the line broadening function (BF) in the optical domain. We show that some interesting clues to the geometry of the BLR can be identified in this way and we apply the results to estimate the physical properties in our sample of AGN.

The paper is organized as follows: in §2 we describe the analytical formalism to extract the profile broadening functions and to calculate the corresponding Gauss-Hermite expansions; in §3 we present our sample and the reduction techniques that we adopted; §4 summarizes our results, with a discussion of the main limits and some indications to improve the analysis; finally our conclusions are given in §5.

2. LINE PROFILE ANALYSIS AND THEORETICAL MODELS

In the effort towards revealing the intrinsic properties of AGN cores, line profile analysis often played a major role. Under specific assumptions about the dynamical conditions within the BLR, such as the hypothesis of virial motions driven by the combined effect of the central engine's gravity and radiation pressure, a number of representative parameters, like the line widths at different intensity levels, or the line asymmetry factors, usually computed in the form of ratios among the line extension toward the blue and red wavelengths, with respect to the line core position, were used in order to describe the profiles and to evaluate the properties of the engine. This kind of approach is prone to the effects of the substantially unknown BLR geometry, with the possibility to introduce systematic misinterpretation of data. Furthermore, it assumes quite specific measurements to be a good approximation of the entire emission line profile, loosing some precious physical details.

In this section we describe a generalized approach to the line profile fitting, already exploited in the past years in the field of advanced stellar kinematics, but adopted for gas kinematics as well (Barton et al. 2000).

2.1. *Emission line broadening from cross-correlation*

The BLR spectrum shows several emission lines corresponding to many permitted and some semi-forbidden transitions of variously ionized atomic species. There are indications that the distribution of the line emitting material is different, according to the ionization potential of the considered emission lines (see e. g. Gaskell & Sparke 1986; Sulentic et al. 1995; Marziani et al. 1996; Snedden & Gaskell 2004; Matsuoka et al. 2008; Mullaney & Ward 2008; Sluse et al. 2008, etc.). Indeed, the interaction of the most energetic AGN radiation with gas probably produces a region where matter is highly ionized. On the contrary, optical shielding effects allow for the survival of low ionization species, in regions where only comparatively low energy photons may penetrate. Therefore, if the BLR structure is such that the shielded component is different from the directly exposed one, the properties of the emission lines will depend on their ionization potential.

On the other hand, choosing to analyze a set of emission lines belonging to a statistical distribution of matter and radiation interactions, it is more likely that the emission regions are not dramatically different. In the optical domain, the Balmer series of hydrogen is the most appropriate choice, because of its strength above the underlying continuum.

Assuming that the Balmer line emission is not affected by large variations across the BLR and introducing the cross-correlation formalism, originally described by Tonry & Davis (1979) and then updated by Statler (1995), we can approximate the observed line spectra as the convolution of an appropriate template of narrow emission lines $T(x)$ with the BLR broadening function $B(x)$:

$$S(x) \simeq T(x) * B(x), \tag{2}$$

where $S(x)$ is the observed spectrum, while x represents a logarithmic wavelength coordinate of the form:

$$x = A \ln \lambda + B, \tag{3}$$

such that the effect of radial velocities results in linear shifts along x. Eq. (2) can be explicitly written as:

$$S(x) \simeq \int T(x) B(x - x') \, \mathrm{d}x' \tag{4}$$

and, if we compute the cross-correlation function of the spectrum with the template, we find:

$$X(x) = S(x) \otimes T(x) = \int S(x) T(x + x') \, \mathrm{d}x'. \tag{5}$$

Using Eq. (4), the cross-correlation function becomes:

$$X(x) \simeq \int \int T(x) B(x - x'') \, \mathrm{d}x'' T(x + x') \, \mathrm{d}x', \tag{6}$$

which, upon changing order of integration, is:

$$X(x) \simeq \int \int T(x) T(x + x') \, \mathrm{d}x' B(x - x'') \, \mathrm{d}x''. \tag{7}$$

Based on the definitions of cross-correlation and convolution, Eq. (7) approximates the cross-correlation function of the spectrum and the template as the convolution of the template autocorrelation function with the object's BF (Statler 1995):

$$X(x) \simeq [T(x) \otimes T(x)] * B(x). \tag{8}$$

Since $T(x)$ is known and $X(x)$ is drawn from observations, as far as the template is correct, it is possible to recover $B(x)$.

Restricting our analysis to the primary cross-correlation peak, which carries most of the kinematical

TABLE 1
List of objects in the sample

Name	RA (hh:mm:ss.s)	Dec (dd:mm:ss)	M_V	z	$FWHM_{H\beta}$ ($km\,s^{-1}$)	Detected in Radio
RX J0801.5+4736	08:01:32.0	+47:36:16	-23.3	0.157	7009 ± 336	Yes
RXS J080358.9+433248	08:03:59.3	+43:32:58	-24.4	0.451	2632 ± 222	No
1RXS J080534.6+543132	08:05:34.9	+54:31:29	-26.5	0.406	3174 ± 299	No
SDSS J081222.99+461529.1	08:12:23.0	+46:15:28	-23.6	0.311	2807 ± 283	No
2MASSi J0816522+425829	08:16:52.3	+42:58:30	-23.1	0.235	3768 ± 186	No
NGC 2639 U10	08:42:30.5	+49:58:03	-23.3	0.305	6046 ± 210	No
SDSS J085632.39+504114.0	08:56:32.4	+50:41:14	-23.9	0.234	2819 ± 157	No
SDSS J085828.69+342343.8	08:58:28.6	+34:23:44	-24.3	0.257	3570 ± 265	No
SDSS J090455.00+511444.6	09:04:55.0	+51:14:44	-23.4	0.224	3620 ± 142	No
RX J0906.0+4851	09:06:01.3	+48:51:48	-24.1	0.390	2503 ± 100	No
RX J0908.7+4939	09:08:47.4	+49:40:07	-24.5	0.421	2137 ± 71	No
1WGA J0931.9+5533	09:32:00.1	+55:33:48	-23.1	0.265	5045 ± 482	Yes
SDSS J093653.84+533126.8	09:36:53.8	+53:31:27	-23.1	0.228	4255 ± 175	No
FIRST J094610.9+322325	09:46:10.9	+32:23:26	-24.5	0.403	1684 ± 235	Yes
KUV 09484+3557	09:51:23.8	+35:42:48	-23.8	0.398	3244 ± 289	No
HS 1001+4840	10:04:13.8	+48:26:06	-24.0	0.562	2962 ± 230	No
PC 1014+4717	10:17:30.9	+47:02:25	-23.7	0.335	2583 ± 103	No
RX J1030.4+5516	10:30:24.9	+55:16:21	-24.8	0.435	2246 ± 157	Yes
FBQS J103359.4+355509	10:33:59.5	+35:55:09	-23.3	0.169	4543 ± 237	Yes
SBS 1047+557B	10:50:55.1	+55:27:23	-24.1	0.333	2253 ± 97	No
RX J1054.7+4831	10:54:44.7	+48:31:39	-24.7	0.286	4428 ± 274	Yes
FBQS J105648.1+370450	10:56:48.2	+37:04:51	-24.1	0.387	4538 ± 272	Yes
FBQS J110704.5+320630	11:07:04.5	+32:06:30	-23.3	0.243	8447 ± 558	Yes
FBQS J112956.5+364919	11:29:56.5	+36:49:19	-24.4	0.399	3564 ± 452	Yes
FBQS J115117.7+382221	11:51:17.8	+38:22:21	-25.4	0.336	3696 ± 242	Yes
RX J1200.4+3334	12:00:28.7	+33:34:43	-23.5	0.284	2864 ± 173	No
RX J1203.8+3711	12:03:54.8	+37:11:37	-23.4	0.401	3725 ± 1020	Yes
1RXS J121759.9+303306	12:17:59.3	+30:33:03	-23.8	0.363	3435 ± 258	No
RX J1218.3+3850	12:18:22.6	+38:50:43	-24.4	0.194	4564 ± 483	No
FBQS J122035.1+385317	12:20:35.1	+38:53:17	-25.3	0.376	1899 ± 164	Yes
FBQS J122424.2+401510	12:24:24.2	+40:15:10	-24.3	0.415	4721 ± 397	Yes
FBQS J122624.2+324429	12:26:24.2	+32:44:29	-23.9	0.242	4535 ± 533	Yes
FBQS J125602.0+385230	12:56:02.0	+38:52:30	-24.1	0.419	1978 ± 147	Yes
FBQS J132515.0+330556	13:25:15.0	+33:05:56	-23.5	0.356	1921 ± 102	Yes
SDSS J144050.77+520446.0	14:40:50.7	+52:04:46	-23.4	0.320	2483 ± 134	No
RX J1452.4+4522	14:52:24.7	+45:22:24	-24.6	0.469	6594 ± 156	Yes
FBQS J145958.4+333701	14:59:58.4	+33:37:01	-25.5	0.644	4389 ± 209	Yes
FIRST J154348.6+401324	15:43:48.7	+40:13:25	-23.4	0.318	5227 ± 391	Yes
SDSS J154833.03+442226.0	15:48:33.1	+44:22:26	-23.5	0.322	3893 ± 343	Yes
FBQS J155147.4+330007	15:51:47.4	+33:00:08	-24.5	0.422	2744 ± 221	Yes

Note. — Together with names and equatorial coordinates (J2000.0), the table lists the absolute magnitude in the V band, the cosmological redshift, $FWHM_{H\beta}$, and a binary flag indicating whether the source is detected in radio or not.

information and it is weakly affected by template mismatch, Eq. (7) can be written in its discrete form, with the simplified notation $F_i = F(x_i)$:

$$X_k \simeq \sum_{i=0}^{N} \left(\sum_{j=0}^{N} T_i\, T_{i+j} \right) B_{k-i}. \qquad (9)$$

Provided that all the functions are null when they are computed outside the range $0 \leq i \leq N$, Eq. (9) defines a system of $N+1$ linear equations in the $N+1$ variables B_{k-i} ($k \geq i$). A standard χ^2-minimization routine can be therefore used to infer the BF of the Balmer lines.

2.2. *Analytical expressions for the broadening functions*

As previously mentioned, the BLR broadening functions are influenced by the effects of complex kinematics within the source and of radiation transfer from the source to the observer. For this reason it is hardly conceivable that a simple analytic expression might be used to fit the resulting profiles. In the case of a geometrically complex distribution of motions in the line emitting region, multiple Gaussian functions provide reasonable fits to the observed profiles. Two Gaussian contributions can usually fit the broad component of Hβ (Popović et al. 2004; Chen et al. 2008), but other contributions, up to five more Gaussians, might be needed to account for the narrow emission lines of Hβ and [O III]. Furthermore, the presence of ordered kinematical components modifies the shape of the BF, raising non-Gaussian features in the profiles.

A good way to estimate the importance of non-Gaussian components is to parameterize the observed BF by means of a Gauss-Hermite orthonormal expansion, similarly to what is described in Van Der Marel & Franx (1993) for the case of stellar kinematics in elliptical galaxies. Following their method, if we call $\alpha(v)$ the normal Gaussian function:

$$\alpha(v) = \frac{1}{\sqrt{2\pi}\sigma_v} \exp\left(-\frac{v^2}{2\sigma_v^2}\right), \qquad (10)$$

where σ_v is the line of sight velocity dispersion, the emission line BF can be expressed as a function of v :

$$B(v) = B_0 \alpha(v - V_{sys}) \left[1 + \sum_{i=3}^{N} h_i H_i(v - V_{sys})\right], \qquad (11)$$

in which we call B_0 the BF normalization factor, V_{sys} the systemic radial velocity offset between the BF and the chosen reference frame, $H_i(v-V_{sys})$ the $i^{\rm th}$ order Hermite polynomial, and h_i the corresponding coefficient. A wide description of the properties of the Hermite polynomials is given in Van Der Marel & Franx (1993). It is demonstrated that odd order functions account for asymmetric distortions of the Gaussian profile, while even order functions have a symmetric effect. Truncating Eq. (11) to $N = 4$, the Hermite polynomials are expressed by:

$$H_3(y) = \frac{1}{\sqrt{6}}(2\sqrt{2}y^3 - 3\sqrt{2}y) \qquad (12a)$$

$$H_4(y) = \frac{1}{\sqrt{24}}(4y^4 - 12y^2 + 3). \qquad (12b)$$

Therefore, it is possible to estimate the role of non-Gaussian kinematical components, using the whole BF profile, simply by fitting the observed shape with a truncated Gauss-Hermite series and measuring the appropriate values of h_3 and h_4.

3. SAMPLE SELECTION AND DATA REDUCTION

3.1. *AGN spectra from SDSS*

To perform our investigation, we needed a homogeneous sample of AGN optical spectra, featuring prominent broad Balmer emission lines. The spectroscopic database of the 6^{th} data release of SDSS (DR6) provides a huge number of objects, whose spectra are collected and processed by a fairly well established standard pipeline (Adelman-McCarthy et al. 2008). In order to collect a set of good signal spectra, we chose to select the sample in the Véron-Cetty catalogue of Quasars and Active Galactic Nuclei (12^{th} Ed.) (Véron-Cetty & Véron 2006), with the following requirements:

- the object redshift had not to exceed the limit $z \approx 0.8$, because objects at larger redshift have their Hβ emission line beyond the SDSS spectral coverage;
- only bright sources, with $M_V < -23$, were considered;
- each object had a spectral classification suggesting the presence of broad emission line profiles;
- the sources are located within the field covered by the SDSS DR6 spectroscopic observations.

On the resulting candidate list, we applied further constraints, that restricted the sample to the most appropriate sources. In particular we chose objects whose spectra had at least three clearly detectable broad Balmer lines and they were not affected by instrumental disturbances or by strong foreground and background contamination. We ended up with a sample of 40 objects that is described in Table 1.

3.2. *Preliminary spectral reduction*

A major advantage in the SDSS database is that it provides spectra with preliminary reduction and calibration, thus simplifying the task of spectral analysis. Therefore, before proceeding with our measurements, we simply had to remove from the spectra those contributions which come from outside the AGN. We applied a correction for Galactic Extinction, estimated by means of a selective extinction function, in the form proposed by Cardelli et al. (1989) with the absorption coefficients evaluated on the basis of the extinction map traced by Schlegel et al. (1998) and available at the NASA Extragalactic Extinction Calculator. We, then, removed the cosmological redshift, bringing the spectra to the rest frame of the narrow [O III] emission lines. Finally, we estimated the host galaxy contamination by applying a spectral decomposition technique, based on the Karhunen-Loéve Transforms described by Connolly et al. (1995) and implemented on SDSS data by Vanden Berk et al. (2006). According to the same method exploited in La Mura et al. (2007), we consider the observed spectra as the linear combinations of principal components, called *eigenspectra*, originated independently by the AGN and its host:

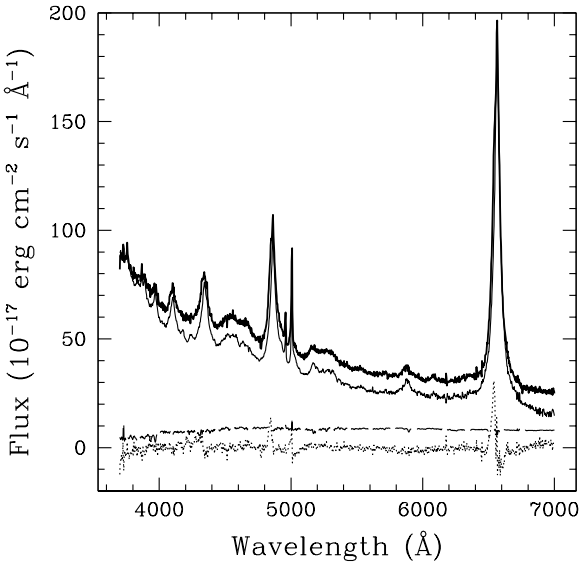

FIG. 1.— Example of spectral decomposition for SDSS J085632.39+504114.0. The observed spectrum, represented by the thick continuous line, is compared with the AGN (thin continuous line) and galactic (long dashed) components. The dotted line in the bottom part of the plot is the fit residual.

$$S(\lambda) = \sum_{i=1}^{n}[q_i \cdot Q_i(\lambda)] + \sum_{j=1}^{m}[g_j \cdot G_j(\lambda)], \qquad (13)$$

with $S(\lambda)$ being the total spectrum, $Q_i(\lambda)$ the $i^{\rm th}$ AGN component, weighted by its coefficient q_i, and $G_j(\lambda)$ the $j^{\rm th}$ host galaxy eigenspectrum associated to the corresponding coefficient g_j. Using the galactic and AGN eigenspectra provided by Yip et al. (2004a,b), we evaluated the coefficients (q_i, g_j) by means of a χ^2-minimization routine involving the first five galaxy eigenspectra and six AGN components. This procedure allows to carry out the separation outlined in Eq. (13), as it is illustrated in Fig. 1, and to subtract an estimate of the host galaxy starlight contaminating the SDSS spectra.

3.3. *Extracting the BLR component*

Once the AGN spectra have been corrected to account for most of the external effects, the task to identify the BLR contribution alone needs the removal of more components, including the underlying continuum of the AGN

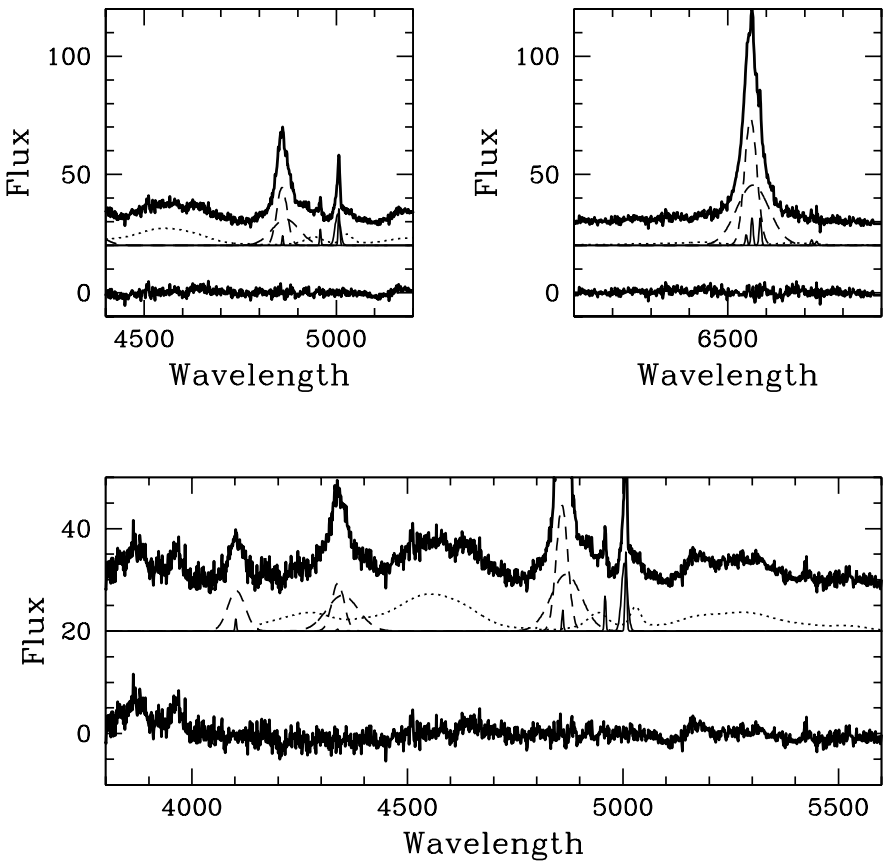

FIG. 2.— Multiple Gaussian decompositions of the profiles of Hβ (upper left panel), Hα (upper right), Hγ, and Hδ (lower panel). Here we use a thick continuous line to plot the continuum subtracted spectrum of PC 1014+4717, a thin continuous line for the estimated NLR contributions, a long dashed line for the BLR components, and a dotted line for Fe II. The thick continuous line in the bottom part of each panel shows the fit residuals, while fluxes and wavelengths are expressed in units of 10^{-17}erg cm^{-2} s^{-1} Å^{-1} and Å, respectively.

central source and the narrow lines coming from the Narrow Line Region (NLR). Measuring the properties of the broad lines, moreover, is often difficult because of the multiple spectral features that are blended together. In the case of the Balmer series, narrow lines from [O III], [N II], [S II], together with the narrow Balmer emissions, have to be taken into account, while blends with broad lines from He II and the multiplets of Fe II can heavily affect the observed profiles.

To subtract the AGN continuum, we fit the spectra with `spline` functions of order ranging from 2 to 5 in wavelength ranges which are usually not affected by prominent lines. The subtraction of narrow lines and the blends with He are dealt with by means of multiple Gaussian profile decompositions, where we use the [O III] emission line at 5007 Å as a template for the other narrow features and we fix the [N II] $\lambda\lambda$ 6548, 6584 emission line ratio to be 1:3. Some special care, instead, is needed in the case of the Fe II multiplets, whose properties have not yet been understood in detail. Following the method suggested by Véron-Cetty et al. (2004), it is possible to remove the Fe II contribution from spectra by scaling and broadening an appropriate template, estimated from the spectrum of an AGN featuring prominent Fe II emission lines. In our work, we used the Fe II template spectrum coming from *I Zwicky* 1 (Botte et al. 2004), splitting it into two parts, which we scaled in order to achieve a better coincidence with our data. The process is summarized in Fig. 2. Most of the steps so far described were carried out with tasks provided in the *IRAF* software package.

Once the removal of contaminating contributions has been performed, we are able to apply the Gauss-Hermite formalism to the profiles of the broad lines so far isolated in the spectra. We perform a first analysis directly on the profiles of the Hβ emission line. The results of this study can be subsequently compared with the shape of the Balmer line broadening functions, which we are now able to infer from the cleaned BLR spectra.

3.4. *The Balmer Line Broadening Functions*

As a result of the previous steps, we now have got a set of BLR Balmer line spectra. Our task is then to recover their BF, by means of the cross-correlation technique outlined in §2.1. To calculate the cross-correlation functions, we build a template of Balmer emission lines, following the median line intensity ratios found by La Mura et al. (2007) in a sample of 90 SDSS spectra of broad line emitting AGN. Our template assumes that the SDSS instrumental profile is a Gaussian function with FWHM = 167 km s^{-1}. At the spectral res-

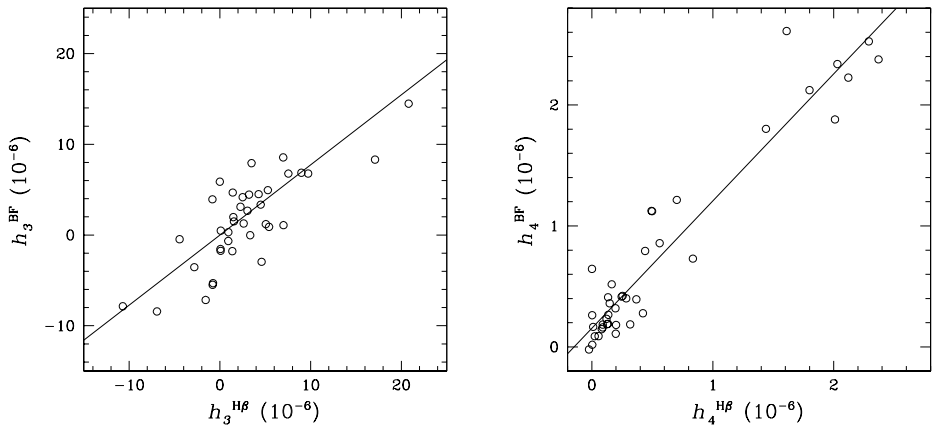

FIG. 3.— Gauss-Hermite expansion coefficients of the line profile BF compared with the same coefficients extracted from the profile of Hβ. The straight lines shown in both panels are the best fit functions described in Eq. (16) and Eq. (17).

olution of Sloan data, the logarithmic sampling of the wavelength coordinate can be performed with discrete bins corresponding to 69 $\mathrm{km\,s^{-1}}$ each. Here we use the *IRAF* task `fxcor` to compute the template autocorrelation function:

$$A(x) = T(x) \otimes T(x) \tag{14}$$

and the cross-correlation functions of the BLR spectra with the template, following the definition of Eq. (5). Again a χ^2-minimization algorithm can be exploited to infer the BF in its discrete form. Applying the least squares formalism to the equation system (9), it follows that the BF of each spectrum must satisfy the relations:

$$\sum_{i=0}^{N} B_i \left(\sum_{j=0}^{N} A_j A_{i-k} \right) = \sum_{i=k}^{N} A_{i-k} X_i. \tag{15}$$

In principle, it is possible to extract an accurate solution for the BF by solving the equation system (15) with $0 \leq k \leq N$. In practice the task is not simple, because it involves the inversion of a coefficient matrix as large as $[(N+1) \times (N+1)]$, with N increasing with the line profile widths up to $N \simeq 400$. However, the complete solution of such a system is not the real purpose of this work, since we are not seeking the detailed shape of the BF, but we are rather looking for the importance of non-Gaussian components. Therefore, we chose to solve the system at lower resolution, interpolating the BF every 8 bins with an analytical profile, which we assumed to be a Gauss-Hermite expansion.

We compared the properties inferred for the BF of our spectra with the results obtained by applying the Gauss-Hermite profile fitting directly to the Hβ emission line. We found that the expansion coefficients in the two cases are highly correlated, supporting a tight relationship among the Hβ emission line profile and the BF of the Balmer series. The details of this comparison are given in Fig. 3, where we plot the values of the expansion coefficients obtained in both ways. As a result, we get:

$$h_3^{\mathrm{BF}} = (0.773 \pm 0.073) h_3^{\mathrm{H}\beta} + (0.721 \pm 0.554) \cdot 10^{-6}, \tag{16}$$

with a correlation coefficient $R = 0.865$ and a null hypothesis $P_0 < 10^{-6}$ and

$$h_4^{\mathrm{BF}} = (1.051 \pm 0.052) h_4^{\mathrm{H}\beta} + (0.154 \pm 0.049) \cdot 10^{-6}, \tag{17}$$

with $R = 0.955$ and $P_0 < 10^{-6}$.

Here we would like to point out that the matrix inversion must be computed only once, because it involves coefficients exclusively drawn from the template autocorrelation function. The cross-correlation functions of the spectra, instead, only affect the known terms of Eq. (15). Hence the advantage of this technique.

3.5. *Spectral property measurements*

After the calculation of the BF of our sample, we performed more measurements of spectral properties in the data, estimating, in particular, the FWHM of the Hβ emission line and the AGN continuum radiation luminosity at 5100 Å. These are needed to infer some of the source physical properties, such as the central black hole mass, its accretion rate and the size of the BLR.

In the case of the line profile measurements, we looked at the Hβ emission line in the BLR spectra, which we previously isolated for cross-correlation with the template. To account for the uncertain continuum and narrow line corrections, we performed five different measurements of the line half width at half the maximum both on the blue and red wing of the line, varying our guess to the continuum and line peak intensity. We combined these estimates to calculate the FWHM, then we averaged them together, and we computed the 1σ dispersion. As a further step, we fit the broad Hβ profile with two Gaussian functions and we applied similar measurements to the identified components.

The optical continuum luminosities at 5100 Å, instead, were evaluated in the AGN spectra that we previously corrected for Galactic Extinction and host contamination. Here, the main source of error arises from the noise fluctuations around the actual signal intensity. For this reason, we assumed the specific continuum luminosity at 5100 Å to be represented by the average luminosity, evaluated in the range running from 5075 Å to 5125 Å, and the associated error to be given by its standard deviation. Therefore, we measured the continuum fluxes of our spectra and we computed the related specific luminosities using the object redshift as a distance indicator, in the framework of a cosmological model defined by $H_0 = 75\,\mathrm{km\,s^{-1}\,Mpc^{-1}}$, $\Omega_{matter} = 0.3$, and $\Omega_\Lambda = 0.7$. A guess to the bolometric luminosity, which is needed to in-

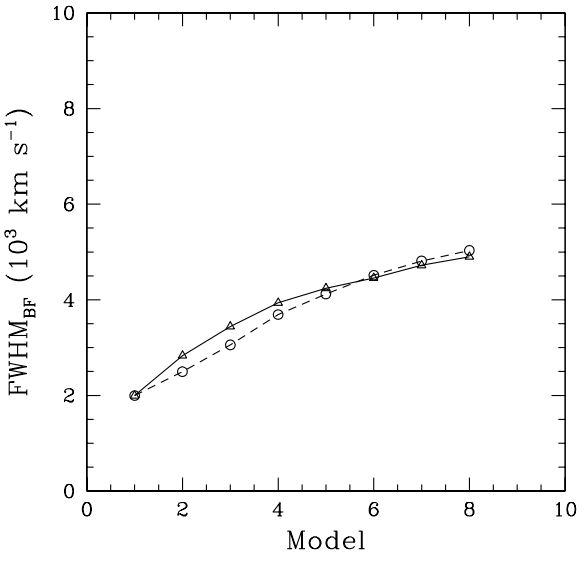

FIG. 4.— Expected FWHM in the BF of emission lines originated in a disk structure. The empty triangles connected by the continuous line are the predicted values for reference disk models with $i = 10°$ in the gravitational field of black holes with M = 1, 2, 4, 6, 8, 10, 12, and 14 $\cdot 10^7 M_\odot$ (respectively models from 1 to 8); the circles with the dashed line show the predicted behavior for the reference disk model in the gravitational field of the black hole with $M = 10^7 M_\odot$, when seen under inclinations of $i = 10°$, 15°, 20°, 25°, 30°, 35°, 40°, and 45° (again from model 1 to 8).

fer the accretion rate onto the central black hole, can be made from the specific luminosity measured in the spectra (e. g. Elvis et al. 1994; but see also Collin et al. 2002; Collin & Kawaguchi 2004, and references therein). Here we assume our objects to have bolometric luminosities approximately given by:

$$L_{bol} \simeq 10 \cdot (5100\,\text{Å} \cdot L_{5100}), \tag{18}$$

where L_{5100} represents our estimate to the continuum specific luminosity at 5100 Å, measured in erg s^{-1} Å^{-1}, and L_{bol} is the bolometric luminosity, given in erg s^{-1}. We note, however, that this assumption is prone to the effect of the large dispersion in the SED of AGN and it may easily introduce an uncertainty of a factor ~ 2, which propagates in the estimated black hole masses and accretion rates.

4. RESULTS AND DISCUSSION

A clear determination of the black hole mass is not possible unless we are able to discriminate the role played by f in Eq. (1). In many circumstances, the black hole mass problem is dealt with through the assumption of a particular geometry, such as a random distribution of virial motions (Netzer 1990; Wandel et al. 1999; Peterson & Wandel 2000), or a flattened rotating system with an inclination mostly inferred by means of statistical considerations (Decarli et al. 2008a). Many authors (Vestergaard et al. 2000; Nikołajuk et al. 2005; Peterson et al. 2004; Sulentic et al. 2006, etc.) pointed out that a considerable flattening is likely to be an intrinsic property of the BLR structure and even that a simple assumption about its inclination may not remove the problem. The very nature of the broad line emitting entities has been investigated extensively (see, for example, Arav et al. 1997, 1998; Laor 2006), leading to the conclusion that the broad line profiles either result from the combination of a large number of emitters, in the order of $\sim 10^7$, or it is produced by motions of a smooth medium. In both cases, it is noticed that a random motion pattern could not be dynamically stable.

With the exception of those objects whose line profiles clearly show double peaks, a strong clue towards an highly inclined rotating system, the BLR inclination is still an open question of crucial importance for determination of black hole mass and accretion rate. Indeed, the assumption of a universal geometrical factor usually leads to the detection of high accretion rates in Narrow Line Seyfert 1 galaxies (NLS1) (e. g. Boller et al. 1996), while adjusting the geometrical factor, according to statistics, affects the black hole masses largely reducing most of the differences. Both these paths might be sources of systematic misunderstandings, therefore a direct and independent measurement of the BLR inclination, or, alternatively, of the black hole accretion rate, would be highly desirable in order to discriminate among the actual dynamical properties and the effect of inclination (Kelly et al. 2008).

A similar test has been performed, for a restricted sample, by Hicks & Malkan (2008) in near infrared spectroscopic observations, leading to the conclusion that the observed gas kinematics is consistent with RM based results for nearly face-on disk structures.

4.1. *Inclination and line profile broadening*

Since the BLR structure cannot be represented by a random motion pattern, the shape of the broad emission lines exhibits large deviations from the Gaussian profile. In the extreme case of the marked double peaks in the spectral lines of Arp 102B, studied by Chen & Halpern (1989), the BLR structure is well explained in terms of the combination of a quasi spherical component with a rotating disk, probably the external accretion disk, seen at an inclination of $i = 32°$. Popović et al. (2004) applied the same model to other single peaked line emitting sources and they found that mildly inclined disks could be responsible for the observed line profiles as well, although uncertainties on the model free parameters might affect the values of the inferred inclinations, as Collin et al. (2006) pointed out.

If the BLR has a flattened component which is seen at low inclination, its emission lines clearly do not exhibit double peaks, but the geometrical structure still modifies the dynamical interpretation of data. We illustrate this concept in Fig. 4, where we plot the expected FWHM in the broadening function of disks surrounding black holes of increasing mass and we compare it to the situation of a black hole of fixed mass, but with the disk seen under different inclinations. It is clear that, within the range of our calculations, there is a mass - inclination degeneracy on the resulting FWHM.

Exploiting the model developed in Chen et al. (1989), Chen & Halpern (1989), and Popović et al. (2004), we computed a range of expected non-Gaussian profiles in the case of a two component BLR structure seen at different inclinations, with a flattened rotating disk and a surrounding distribution of gas, giving rise to a bell-shaped contribution. In its original purpose, this model was conceived to fit the properties of an accretion disk, introducing some free parameters for the disk radii, in-

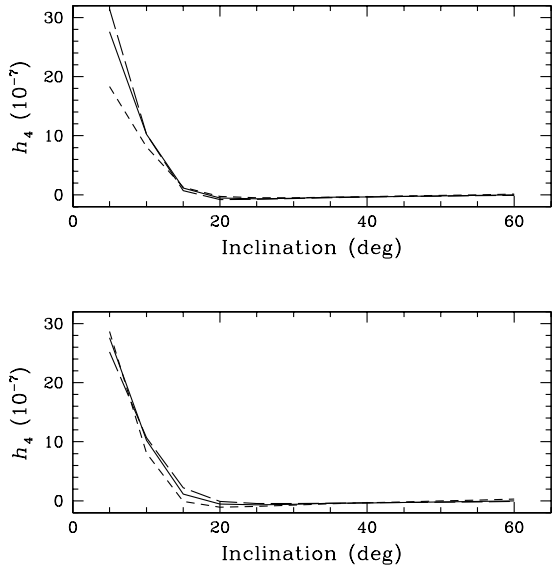

FIG. 5.— Comparison of the reference model predictions concerning the broadening function kurtosis (continuous lines) with four variants: in the upper panel we plot models with stronger (long dashed line) and weaker (short dashed line) disk emission with respect to the bell-shaped component; in the bottom panel we show the differences obtained by setting $\sigma_{Bell} = 0.07c$ (short dashed line) and $\sigma_{Bell} = 0.09c$ (long dashed line).

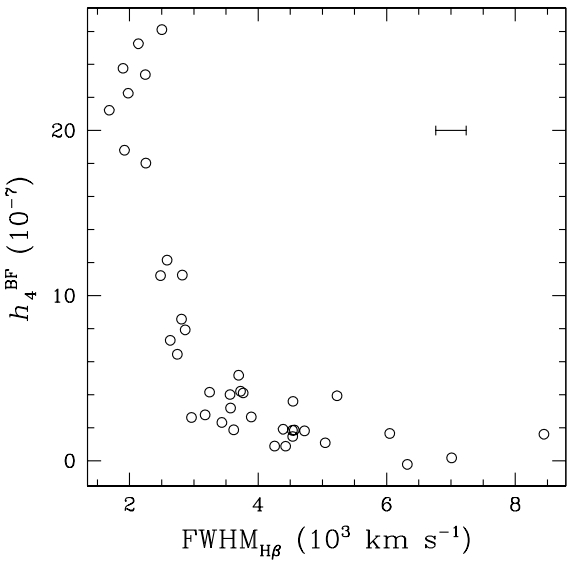

FIG. 6.— BF kurtosis plotted as a function of FWHM$_{H\beta}$. We observe a large evolution of the line profile kurtosis as a function of broadening, suggesting the possibility of inclination effects in nearly face-on flattened structures. Such effects become weaker as the profile width increases.

trinsic velocity dispersion, and line emission. Adjusting these parameters, it would be possible to fit the broad emission line profiles of possibly all the spectra of our sample, but reasonable fits can be obtained in several ways, without tightly constraining the physical properties of the BLR. Here we try to predict the effect of a flattened BLR component on the observed line profiles, therefore we fix some of these parameters on the basis of the results collected by La Mura et al. (2007). Our reference model assumes $R_{in} = 1834R_S$ for inner radius, $R_{BLR} = 18340R_S$ for outer radius, $\sigma_{Disk} = 0.003c$ as the intrinsic velocity dispersion in the disk, and $\alpha = -2.0$ for the radial emission power law, where R_S and c represent the Schwarzshild radius and the speed of light. Moreover, this model includes a bell-shaped gas distribution having a velocity dispersion of $\sigma_{Bell} = 0.008c$. The reference model carries out the best match to the observed line profiles with the assumption of various disk inclinations.

In Fig. 5, we compare the reference model with some variants, obtained with slightly different parameters. We note that all the models predict a strong dependence of the line profile kurtosis (the coefficient h_4 in the Gauss-Hermite expansion) on the disk inclination, in the range of small values of i. The reason is quite simple, because a nearly face-on disk enhances the low radial velocity peak of the BF, increasing the kurtosis of the profile, while an edge-on disk is more likely to affect the high velocity wings. However, differences in the relative normalization of the bell-shaped component, with respect to the disk, or in its intrinsic velocity dispersion, may also affect the inferred kurtosis. The assumed strength of the bell-shaped component has a large effect on the predicted kurtosis for $i \leq 10°$, while its velocity dispersion has a weaker influence in the range $10° \leq i \leq 20°$. Since large changes in the model parameters quickly result in predictions that do not match the observed line profiles, we assume, in our calculations, a confidential uncertainty of $\Delta i = \pm 2°$, for $i \leq 10°$, and of $\Delta i = \pm 5°$, for $i > 10°$, where the dependence of kurtosis on inclination becomes shallower. At $i \geq 20°$ the kurtosis is no longer a useful indicator of inclination.

As we show in Fig. 6, however, where we plot the measured values of h_4 as a function of FWHM$_{H\beta}$, there is a remarkable evolution of the line profile kurtosis, which decreases for increasing line profile width. Such an effect is a clear indication that a considerable variation of the geometrical factor f might be present and it should be taken into account in order to estimate the actual properties of the SMBH located in the centre. Using the model predictions, we can exploit the broad line kurtosis to estimate the inclination of the flattened BLR component and to apply a correction to our dynamical interpretation of the observed line profiles. It should be noted, however, that, although the kurtosis is estimated from the whole profile, it reduces the available information to a single parameter. It is, therefore, very important that the model provides a good fit of the observed line profiles.

4.2. *Mass and accretion rate estimates*

It can be shown that completely neglecting the role played by the BLR geometrical factor may lead to incorrect black hole mass estimates, with uncertainties that, in the worst cases, could span over two orders of magnitude. This problem is particularly important in the case of NLS1 galaxies, whose nature has been carefully investigated, to find out whether they are characterized by flattened rotating structures seen at low inclination (Osterbrock & Pogge 1985), or they are actually low mass black holes accreting at very high rates, sometimes well beyond the Eddington limit, as it is discussed, for

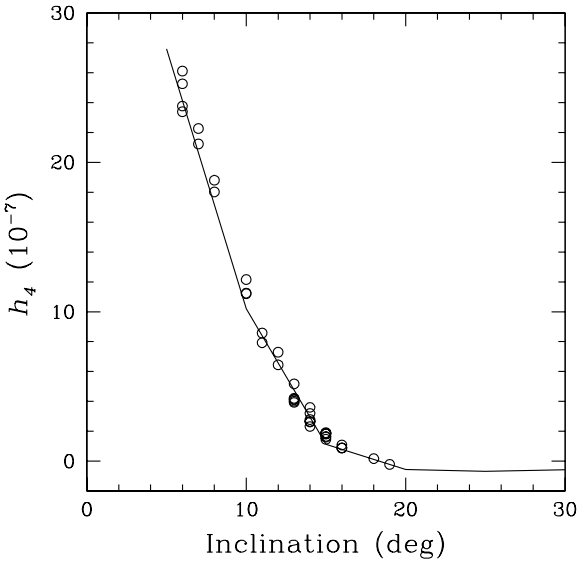

FIG. 7.— BLR inclination inferred by comparison among the BF kurtosis, predicted by the reference model for various inclinations, and the corresponding distribution observed in our data. According to the model predictions, the BF kurtosis is very sensitive to flattening and inclination in nearly face-on structures, while it becomes a weaker indicator for larger inclinations.

instance, in Boller et al. (1996) or in Komossa (2008). Moreover, the role played by non gravitational forces, especially in the case of high radiative efficiency, may also influence the kinematical properties of gas, as suggested by Marconi et al. (2008), affecting the reliability of the virial assumption. In their work, La Mura et al. (2007) found that, although NLS1 had quite high accretion rates, they were not exceptional with respect to other AGN in the sample, a result echoed by the considerations of Decarli et al. (2008a).

On the other hand, while Shemmer et al. (2006) argue that X-ray observations may provide a direct clue to the black hole accretion rate and thus remove the degeneracy introduced by the $\mathrm{FWHM}_{\mathrm{H}\beta}$ dependent mass estimates, Decarli et al. (2008b) and Labita et al. (2006) use the black hole correlations with the host properties, identified by Ferrarese et al. (2000, 2006), to calibrate the geometrical factor. Both methods suggest that some care should be taken in using only the profile of Hβ to infer the physical properties of AGN.

With the information coming from the line profile distortions, we compute our estimates of the black hole mass and accretion rate by introducing an *equivalent velocity field*, defined by:

$$v_{eq} = \frac{1}{2}\left[\frac{\sqrt{3}}{2}\mathrm{FWHM}_{Bell}(\mathrm{H}\beta) + \frac{\mathrm{FWHM}_{Disk}(\mathrm{H}\beta)}{4\sin i}\right]. \quad (19)$$

Assuming that the line profile broadening results from both planar and non-planar motions (Labita et al. 2006; McLure et al. 2002; Jarvis & McLure 2006, etc.), v_{eq} combines the velocity estimates obtained from the Hβ emission line profile by fitting two Gaussian functions, which are subsequently compared with the reference model, providing a distinction among the bell-shaped and the flattened contributions. The corresponding geometrical factors are assumed to be, respectively, the classical interpretation of Netzer (1990) and that of a rotating disk, confined in a smaller region with respect to the other component. The inclination of the disk is estimated by comparison of the BF kurtosis with that of the reference model, as shown in Fig. 7, and its characteristic radius is assumed to be approximately four times smaller than the typical size of the bell-shaped component. To calculate the black hole mass, we introduce v_{eq} in Eq. (1), bringing the geometrical factor into the modified velocity field, and we estimate the corresponding Eddington ratio from the bolometric luminosity in Eq. (18).

The results of our measurements and calculations are summarized in Table 2, together with the computed uncertainty ranges. Our method breaks the strong dependence of the black hole accretion rate and mass estimates on the width of Hβ since it exploits more indications, coming from the broadening functions of the observed Balmer lines. Moreover, the typical inclinations inferred for the BLR of our spectra are consistent with those estimated by Popović et al. (2008), suggesting that this situation is quite common in single peaked broad line emitters. Table 2, however, does not include the errors which could be introduced by our assumptions, concerning the source luminosity and the BLR structure. Such uncertainties may be as large as a factor of 2 or 3, as seen in the AGN SED distribution, or by adopting different structural models for the BLR. We shall further discuss the role of these uncertainties with the help of some consistency checks.

4.3. *Discussion*

While our estimates of bolometric luminosity and, consequently, black hole mass and accretion rate are essentially scaled by our measurement of the optical continuum luminosity, the dynamical interpretation of the line profiles still suffers from undeniable shortcomings. Adopting a two component model to explain the line profile broadening complicates the relationship among $\mathrm{FWHM}_{H\beta}$ and the black hole mass, introducing a geometrical factor which depends on the inclination of the flattened component and on its relative importance with respect to the BLR as a whole. Because disks are the most viable solution to support accretion flows in presence of angular momentum, numerous authors suggested that the broad line gas could originate in the disks themselves (e. g. Shields 1977; Shlosman et al. 1985; Emmering et al. 1992). Models based on accretion disks only, however, have great difficulties in accounting for AGN observational properties (see Kinney 1994, for example). The assumption of a two component model improves our ability to understand the observed line profiles, but it still fails in placing strong constraints on the structure of the BLR, since the origin of the bell-shaped component is not clear. Indeed, there are models, such as those of Collin-Souffrin & Dumont (1990), Jackson et al. (1991), or Murray & Chiang (1997), which achieve a good match with observations on more physical grounds, either exploiting very large disk radii, or computing the effect of radiation transfer across radial gas flows close to the disk. Clearly, the choice of different models affects the interpretation of AGN dynamical properties and this is a major concern in the

TABLE 2
Estimated properties of the sources

Name[a]	L_{bol} (10^{44}ergs^{-1})	h_3 (10^{-7})	h_4 (10^{-7})	i (deg)	M_{BH} ($10^8 M_\odot$)	L_{bol} / L_{Edd}
RX J0801.5+4736⋆	20 ± 1	3.1	0.2	18	14 ± 5	0.011 ± 0.004
RXS J080358.9+433248	36 ± 2	8.9	7.3	12	5 ± 2	0.054 ± 0.027
1RXS J080534.6+543132	83 ± 2	-71.6	2.8	14	8 ± 3	0.083 ± 0.032
SDSS J081222.99+461529.1	37 ± 1	68.6	8.6	11	10 ± 4	0.028 ± 0.013
2MASSi J0816522+425829	25 ± 1	-0.3	4.1	13	9 ± 4	0.021 ± 0.010
NGC 2639 U10	17 ± 1	46.8	1.7	15	4 ± 1	0.031 ± 0.012
SDSS J085632.39+504114.0	39 ± 1	39.3	11.2	10	5 ± 3	0.057 ± 0.036
SDSS J085828.69+342343.8	37 ± 1	-15.4	3.2	14	7 ± 3	0.038 ± 0.016
SDSS J090455.00+511444.6	19 ± 1	45.0	1.9	15	7 ± 3	0.021 ± 0.009
RX J0906.0+4851	35 ± 1	197.8	26.1	6	13 ± 7	0.020 ± 0.011
RX J0908.7+4939	87 ± 2	83.1	25.3	6	14 ± 6	0.048 ± 0.023
1WGA J0931.9+5533⋆	26 ± 1	-4.7	1.1	16	32 ± 9	0.006 ± 0.002
SDSS J093653.84+533126.8	25 ± 1	-54.9	0.9	16	36 ± 12	0.005 ± 0.002
FIRST J094610.9+322325⋆	31 ± 2	-161.1	21.2	7	5 ± 2	0.048 ± 0.021
KUV 09484+3557	22 ± 1	49.4	4.1	13	5 ± 2	0.037 ± 0.017
HS 1001+4840	24 ± 3	58.8	2.6	14	12 ± 4	0.016 ± 0.008
PC 1014+4717	25 ± 1	85.5	12.1	10	5 ± 3	0.038 ± 0.023
RX J1030.4+5516⋆	40 ± 4	144.8	23.4	6	12 ± 6	0.026 ± 0.016
FBQS J103359.4+355509⋆	13 ± 1	26.7	3.6	14	3 ± 1	0.030 ± 0.010
SBS 1047+557B	43 ± 2	44.6	18.0	8	8 ± 3	0.039 ± 0.016
RX J1054.7+4831⋆	49 ± 2	31.1	0.9	16	12 ± 5	0.030 ± 0.013
FBQS J105648.1+370450⋆	20 ± 2	19.8	1.5	15	5 ± 2	0.028 ± 0.014
FBQS J110704.5+320630⋆	18 ± 1	-35.5	1.6	15	24 ± 11	0.006 ± 0.003
FBQS J112956.5+364919⋆	10 ± 1	67.7	4.0	13	1.8 ± 0.7	0.041 ± 0.020
FBQS J115117.7+382221⋆	188 ± 4	-17.8	5.2	13	22 ± 8	0.065 ± 0.026
RX J1200.4+3334	9 ± 1	10.8	7.9	11	3 ± 1	0.023 ± 0.014
RX J1203.8+3711⋆	27 ± 2	79.2	4.2	13	3 ± 2	0.068 ± 0.041
1RXS J121759.9+303306	17 ± 1	33.4	2.3	14	5 ± 2	0.025 ± 0.013
RX J1218.3+3850	15 ± 1	-17.4	1.9	15	6 ± 3	0.018 ± 0.009
FBQS J122035.1+385317⋆	93 ± 2	-84.3	23.8	6	9 ± 4	0.079 ± 0.040
FBQS J122424.2+401510⋆	35 ± 2	15.0	1.8	15	8 ± 2	0.035 ± 0.013
FBQS J122624.2+324429⋆	7 ± 1	12.7	1.8	15	3 ± 1	0.016 ± 0.007
FBQS J125602.0+385230	31 ± 3	-78.5	22.3	7	4 ± 2	0.054 ± 0.032
FBQS J132515.0+330556	27 ± 1	-29.5	18.8	8	5 ± 2	0.039 ± 0.017
SDSS J144050.77+520446.0	20 ± 1	67.7	11.2	10	6 ± 3	0.028 ± 0.016
RX J1452.4+4522⋆	88 ± 4	4.8	-0.2	19	6 ± 2	0.105 ± 0.044
FBQS J145958.4+333701⋆	89 ± 20	41.7	1.9	15	8 ± 4	0.081 ± 0.056
FIRST J154348.6+401324⋆	29 ± 2	-53.0	3.9	13	5 ± 2	0.042 ± 0.016
SDSS J154833.03+442226.0⋆	23 ± 1	-6.6	2.6	14	8 ± 3	0.021 ± 0.009
FBQS J155147.4+330007⋆	32 ± 3	12.0	6.4	12	3 ± 2	0.070 ± 0.039

Note. — This table reports the bolometric luminosities, the Gauss-Hermite expansion coefficients for the BF profile, the inferred inclination, and an estimate of the central black hole mass and accretion rate.
[a] Objects marked with a ⋆ have a polarization measurement in the NVSS catalogue.

case of the BLR.

A particularly important problem, involving the determination of AGN physical properties from emission lines, resides in the line profile asymmetries. Several factors, such as partial obscuration, geometrical structure, or large scale non-virialized motions can produce asymmetric line profiles. Moreover, relativistic effects within the gravitational field of the SMBH give raise to asymmetries, especially in the high velocity wings of the profile, which are included in the calculations of the model by Chen & Halpern (1989). In order to assess how much the asymmetric component affects our estimates of the velocity field, we introduced an asymmetry parameter:

$$K_3 = h_3 H_3(\mathrm{HWHM}_{\mathrm{H}\beta}), \qquad (20)$$

expressing the relative contribution of the asymmetric component, with respect to the Gaussian component, in the profile of Hβ at its half-maximum level. As we show in Fig. 8, the asymmetric component gives a contribution to the FWHM which rarely exceeds the 10% level. The most extreme cases, where the asymmetric component becomes larger than 20%, occur only in the range of very broad line emitting sources. Although this does not appear to be a general property of broad line objects, it echoes the observation of larger asymmetries in objects where $\mathrm{FWHM}_{\mathrm{H}\beta} > 4000\,\mathrm{km\,s^{-1}}$, which is among the features identified by Sulentic et al. (2000, 2006) in their distinction between Population A and B sources. Objects with the largest asymmetries are more problematic for the comparison with the reference model, used to calculate the equivalent velocity field in the BLR. However, comparing their masses and accretion rates with those of the other sources, we do not find systematic differences that could suggest the need for specific model corrections in the asymmetric line emitters, as it is shown in Fig. 9. Here we see that the result of introducing the BLR inclination in our calculations is to remove the strong dependence of the accretion rate on $\mathrm{FWHM}_{\mathrm{H}\beta}$, that was commonly found with isotropic mass estimates. Instead, we are left with a much more complex situation, where, though a slight trend to measure lower accretion rates in broad line emitting sources is still present, it is not a universal condition. An inverse power law fit to the data yields $L_{bol}/L_{Edd} \propto \mathrm{FWHM}_{\mathrm{H}\beta}{}^{-0.75}$, considerably weaker than the old isotropic prediction of

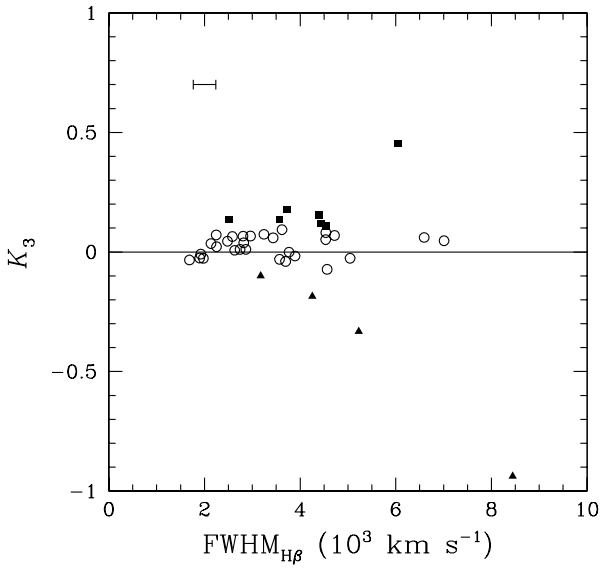

FIG. 8.— Hβ asymmetry parameter distribution with respect to FWHM$_{H\beta}$. Filled symbols represent objects where the asymmetric component exceeds 10% of the Gaussian contribution. We plot as triangles objects that are affected by negative asymmetry, yielding blue shifted peaks and red shifted wings, and squares for positive asymmetry sources, having a red shifted peak with blue shifted wings. Large asymmetries characterize objects where fits with the reference model are more likely to be problematic. The bar in the upper left region of the diagram is a median estimate of the measurement errors.

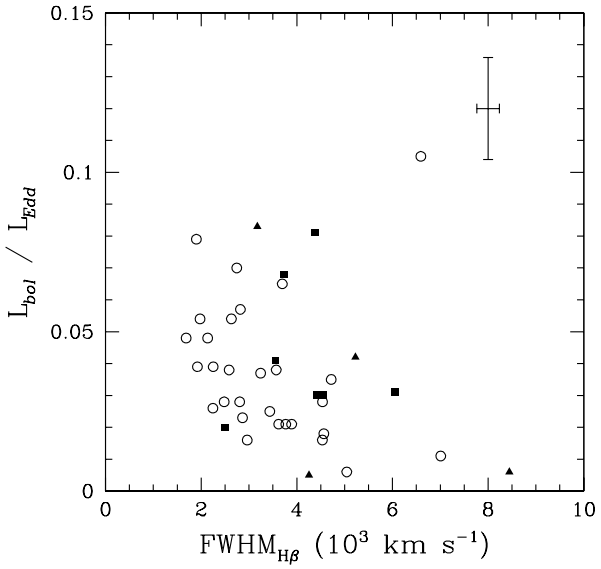

FIG. 9.— SMBH accretion rates as a function of FWHM$_{H\beta}$, with the same symbols as in Fig. 8. The cross in the upper right region of the diagram is the median uncertainty of measurements. We do not detect either dramatic accretion rate excesses or systematic trends associated to the line width, although higher accretion rates appear to be more common in the domain of narrow emission line sources. This conclusion seems not to be affected by asymmetric line profiles.

$L_{bol}/L_{Edd} \propto$ FWHM$_{H\beta}{}^{-2}$. In particular, we do not observe dramatic excesses in the accretion rate of our sources, whose estimates are far below the corresponding Eddington limits.

Most of the results achieved in this work depend critically on the choice of our reference model, which leads us to conclude that the BLR has a flattened component, that is commonly seen at $i \leq 20°$. In the case of radio-loud sources, nearly face-on disk structures are likely to produce a radio jet oriented along our line of sight towards the object, and the resulting signal should be highly variable and polarized. Although we were not able to find any information about variability, some of the radio loud sources in our sample have been detected in the NRAO VLA Sky Survey (NVSS), which provides measurments of the radio flux and polarization at the frequency of 1.4 GHz (Condon et al. 1998).[4] We identify these objects in Table 2 and we compare the degree of linear polarization with our inclination estimates in Fig. 10. Although the uncertainties are quite large, a significant degree of linear polarization is detected in many objects and it appears to be an averagely decreasing function of i.

A comparison of our mass determinations with the old isotropic assumption allows us to study the properties of the geometrical factor within our sample. The situation depicted in Fig. 11 clearly indicates that significant effects, up to a factor ~ 30, should be expected and that they are more commonly observed in the range of sources with FWHM$_{H\beta} \leq 3000 - 4000$km s^{-1}. We find that the average value of the geometrical factor for black hole mass determinations based on FWHM$_{H\beta}$ is $f = 10.58 \pm 7.70$, marginally consistent with the result achieved by Onken et al. (2004), who gave $f = 5.5 \pm 1.9$ using the emission line dispersions.

[4] Polarization data are available at http://www.cv.nrao.edu/nvss/NVSSlist.shtml

5. CONCLUSIONS

In this work we investigated the shape of the emission line broadening function in the BLR of active galactic nuclei. We used a technique based on cross-correlation and Gauss-Hermite line profile fitting, applied to the Balmer series, to infer the broadening functions and we compared them with the predictions of a structural model for the BLR. According to our results, we come to the following conclusions:

- the line profile broadening functions carry much detailed information about kinematics of the BLR, which can be better understood by means of techniques exploiting the whole profile, rather than restricting on specific parameters;
- the observed distribution of line profile kurtosis is consistent with the presence of a flattened component in the BLR, with a typical inclination $i \leq 20°$, though the actual values of i may depend on the adopted model;
- some of the objects included in the sample have quoted measurments of linear polarization at radio frequencies, which averagely increase as the estimated BLR inclination approaches face-on;
- correcting the SMBH mass and accretion rate estimates for geometry reduces the anti-correlation among FWHM$_{H\beta}$ and accretion rate to a much weaker trend;

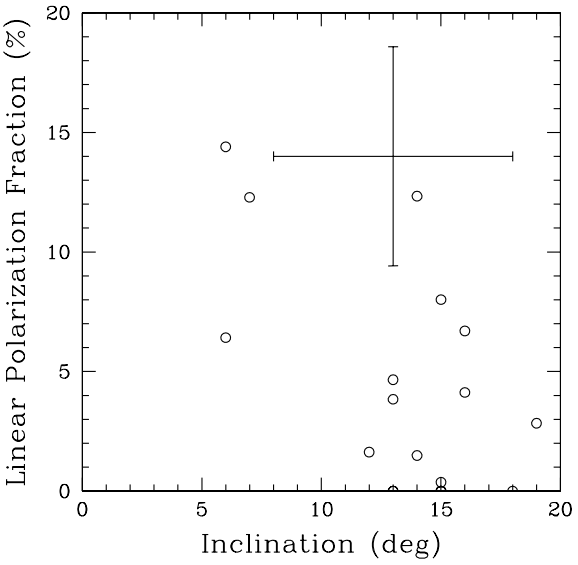

FIG. 10.— Degree of linear polarization at the radio frequency of 1.4 GHz as a function of the inferred BLR inclination. The cross in the upper left corner gives the median uncertainty estimate. Polarization data are from the NVSS catalogue.

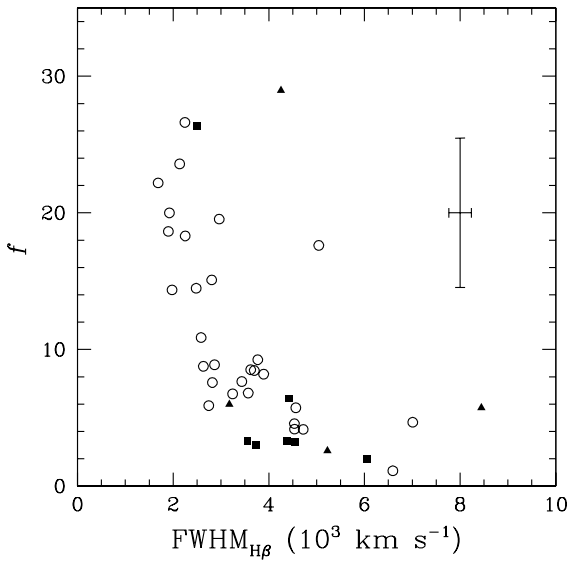

FIG. 11.— Geometrical factors obtained by comparison of the virial product of Eq. (1) and our black hole mass estimates, with the same symbols as in Fig. 8. The effect of the geometrical factor is generally stronger as the line profile width decreases, with a correction to the black hole mass estimate which can be as high as a factor of ~ 30.

- there are no particular indications, in our results, for a strong influence of the line profile asymmetries on the determination of the SMBH properties.

Although this analysis may represent an advance in the problem of determining the role of the BLR geometrical factor, more questions should be answered, concerning how the two components combine in the observed line profiles. A precious contribution in this effort would probably result from the comparison of this technique with some independent way to estimate the black hole accretion rate. Recent works suggested that this test could be possible, for example, with X-ray observations. The ability to constrain the BLR geometrical factor, then, could be applied to study the properties of black hole - host galaxy scaling relations with improved accuracy.

We thank the anonymous referee for useful suggestions and discussion leading to significant improvement of this work.

L. Č. Popović was supported by the Ministry of Science of R. Serbia through project 146002 "Astrophysical Spectroscopy of Extragalactic Objects."

Funding for the SDSS and SDSS-II has been provided by the Alfred P. Sloan Foundation, the Participating Institutions, the National Science Foundation, the U.S. Department of Energy, the National Aeronautics and Space Administration, the Japanese Monbukagakusho, the Max Planck Society, and the Higher Education Funding Council for England. The SDSS Web Site is http://www.sdss.org/.

The SDSS is managed by the Astrophysical Research Consortium for the Participating Institutions. The Participating Institutions are the American Museum of Natural History, Astrophysical Institute Potsdam, University of Basel, University of Cambridge, Case Western Reserve University, University of Chicago, Drexel University, Fermilab, the Institute for Advanced Study, the Japan Participation Group, Johns Hopkins University, the Joint Institute for Nuclear Astrophysics, the Kavli Institute for Particle Astrophysics and Cosmology, the Korean Scientist Group, the Chinese Academy of Sciences (LAMOST), Los Alamos National Laboratory, the Max-Planck-Institute for Astronomy (MPIA), the Max-Planck-Institute for Astrophysics (MPA), New Mexico State University, Ohio State University, University of Pittsburgh, University of Portsmouth, Princeton University, the United States Naval Observatory, and the University of Washington.

REFERENCES

Adelman-McCarthy, J. K. Agueros, M. A., Allam. S. S., et al. 2008, ApJS, 175, 297
Arav, N., Barlow, T. A., Laor, A., & Blandford, R. D. 1997, MNRAS, 288, 1015
Arav, N., Barlow, T. A., Laor, A., Sargent, W. L. W., & Blandford, R. 1998, MNRAS, 297, 990
Barton, E., Kannappan, S. J., Kurtz, M. J., & Geller, M. J. 2000, PASP, 112, 367
Bentz, M. C., Peterson, B. M., Pogge, R. W., Vestergaard, M., & Onken, C. A. 2006, ApJ, 644, 133
Blandford, R. D. & McKee, C. F. 1982, ApJ, 255, 419
Boller, T., Brandt, W. N., & Fink, H. 1996, A&A, 305, 53
Botte, V., Ciroi, S., Rafanelli, P., & Di Mille, F. 2004, AJ, 127, 3168
Capriotti, E., Foltz, C., & Byard, P. 1980, ApJ, 241, 903
Capriotti, E., Foltz, C., & Byard, P. 1981, ApJ, 245, 396
Cardelli, J. A., Clayton, G. C., & Mathis, J. S. 1989, ApJ, 345, 245
Chen, K. & Halpern, J. P. 1989, ApJ, 344, 115
Chen, K., Halpern, J. P., & Filippenko, A. V. 1989, ApJ, 339, 742
Chen, H., Wang, J.-M., Ho, L. C., Chen, Y.-M., Bian, W.-H., & Xue, S.-J. 2008, ApJL, 683, 115
Collin, S., Boisson, C., Mouchet, M., Dumont, A.-M., Coupé, S., Pourquet, D., & Rokaki, E. 2002, MNRAS, 388, 771
Collin, S. & Kawaguchi, T. 2004, MNRAS, 426, 797

Collin, S., Kawaguchi, T., Peterson, B. M., & Vestergaard, M. 2006, A&A, 456, 75
Collin-Souffrin, S. & Dumont, A. M. 1990, MNRAS, 229, 292
Condon, J. J., Cotton, W. D., Greisen, E. W., Yin, Q. F., Perley, R. A., Taylor, G. B., & Broderick, J. J. 1998, AJ, 115, 1693
Connolly, A. J., Szalay, A. S., Bershady, M. A., Kinney, A. L., & Calzetti, D. 1995, AJ, 110, 1071
Decarli, R., Dotti, M., Fontana, M., Haardt, F. 2008a, MNRAS, 386, 15
Decarli, R., Labita, M., Treves, A., Falomo R. 2008b, MNRAS, 387, 1237
Elvis, M., Wilkes, B. J., McDowell, J. C., Green, R. F., Bechtold, J., Willner, S. P., Oey, M. S., Polomski, E., & Cutri, R. 1994, ApJS, 95, 1
Emmering, R. T., Blandford, R. D., & Shlosman, I. 1992, ApJ, 385, 460
Ferland, G. J., Peterson, B. M., Horne, K., Welsh, W. F., & Nahar, S. N. 1992, ApJ, 387, 95
Ferrarese, L. & Merritt, D. 2000, ApJ, 539, 9
Ferrarese, L., Côté, P., Dalla Bontà, E., Peng, E. W., Merritt, D., Jordán, A., Blakeslee, J. P., Haşegan, M., Mei, S., Piatek, S., Tonry, J. L., West, M. J. 2006, ApJ, 644, 21
Gaskell, C. M. & Sparke, L. S. 1986, ApJ, 305, 175
Hicks, E. K. S. & Malkan, M. A. 2008, ApJS, 174, 31
Jackson, N, Penston, M. V., & Pérez, E. 1991, MNRAS, 249, 577
Jarvis, M. J. & McLure, R. J. 2006, MNRAS, 369, 182
Kaspi, S., Smith, P. S., Netzer, H., Maoz, D., Jannuzi, B. T., & Giveon, U. 2000, ApJ, 533, 631
Kaspi, S., Maoz, D., Netzer, H., Peterson, B. M., Vestergaard, M., & Jannuzi, B. T. 2005, ApJ, 629, 61
Kaspi, S., Brandt, W. N., Maoz, D., Netzer, H., Schneider, D. P., Shemmer, O. 2007, ApJ, 659, 997
Kellermann, K. I., Vermeulen, R. C., Zensus, J. A., Cohen, M. H. 1998, AJ, 115, 1295
Kelly, B. C., Bechtold, J. 2007, ApJS, 168, 1
Kelly, B. C., Bechtold, J., Trump, J. R., Vestergaard, M., & Siemiginowska, A. 2008, ApJS, 176, 355
Kinney, A. L. 1994, in ASP Conf. Ser. 54, The First Stromlo Symposium : The Physics of Active Galaxies, ed. B. V. Bicknell, M. A. Dopita, & P. J. Quinn, 61
Komossa, S. 2008, The Nuclear Region, Host Galaxy and Environment of Active Galaxies, ed. Benítez E., Cruz-González I., & Krongold Y., RevMexAA (SC) Vol. 32, 86
Korista, K. T. & Goad, M. R. 2004, ApJ, 606, 749
Labita, M., Treves, A., Falomo, R., & Uslenghi, M. 2006, MNRAS, 373, 551
La Mura, G., Popović, L. Č., Ciroi, S., Rafanelli, P., & Ilić, D. 2007, ApJ, 671, 104
Laor, A., Barth, A. J., Ho, L. C., & Filippenko, A. V. 2006, ApJ, 636, 83
Laor, A. 2007, in ASP Conf. Ser. 373, The Central Engine of Active Galactic Nuclei, ed. L. C. Ho & J.-W. Wang (San Francisco: ASP), 384
Marconi, A., Axon, D. J., Maiolino, R., Nagao, T., Pastorini, G., Pietrini, P., Robinson, A., Torricelli, G. 2008, ApJ, 678, 693
Marziani, P., Sulentic, J. W., Dultzin-Hacyan, D., Calvani, M., & Moles, M. 1996, ApJS, 104, 37
Marziani, P., Dultzin-Hacyan, D., Sulentic, J. W. 2006, New Development in Black Hole Research (New York: Nova Science Publishers)
Matsuoka, Y., Kawara, K., & Oyabu, S. 2008, ApJ, 673, 62
McGill, K. L., Woo, J.-H., Treu, T., Malkan, M. A. 2008, ApJ, 673, 703
McLure, R. J. & Dunlop, J. S. 2002, MNRAS, 331, 795
Mullaney, J. R. & Ward, M. J. 2008, MNRAS, 385, 53
Murray, N. & Chiang, J. 1997, ApJ, 474, 91
Netzer, H. 1990 in Active Galactic Nuclei, ed. R. D. Blandford, H. Netzer, & L. Woltjer (Berlin: Springer) 137
Nikołajuk, M., Czerny, B., & Ziólkowsky, J. 2005 in AIP Conf. Proc. 801, Astrophysical Sources of High Energy Particles and Radiation, ed. T. Bulik, B. Rudak, & G. Madejski (Melville: AIP), 220
Onken, A. C., Ferrarese, L., Merritt, D., Peterson, B. M., Pogge, R. W., Vestergaard, M., & Wandel, A. 2004, ApJ, 615, 645
Osterbrock, D. E. & Pogge, R. W. 1985, ApJ, 297, 166
Osterbrock, D. E. 1989, Astrophysics of Gaseous Nebulae and Active Galactic Nuclei (1st ed.; Sausalito: University Science Books)
Peterson, B. M. & Wandel, A. 1999, ApJ, 521, 95
Peterson, B. M. & Wandel, A. 2000, ApJ, 540, 13
Peterson, B. M., Ferrarese, L., Gilbert, K. M., Kaspi, S., Malkan, M. A., Maoz, D., Merritt, D., Netzer, H., Onken, C. A., Pogge, R. W., Vestergaard, M., Wandel, A. 2004, ApJ, 613, 682
Popović, L. Č., Mediavilla, E., Bon, E., & Ilić, D. 2004, A&A, 423, 909
Popović, L. Č., Bon, E., Gavrilović, N. 2008, The Nuclear Region, Host Galaxy and Environment of Active Galaxies, ed. Benítez E., Cruz-González I., & Krongold Y., RevMexAA (SC) Vol. 32, 99
Schlegel, D. J., Finkbeiner, D. P., & Davis, M. 1998, ApJ, 500, 525
Shemmer, O., Brandt, W. N., Netzer, H., Maiolino, R., Kaspi, S. 2006, ApJ, 646, 29
Shields, G. A. 1977, ApL, 18, 119
Shlosman, I., Vitello, P. A., & Shaviv, G. 1985, ApJ, 294, 96
Sluse, D., Claeskens, J.-F., Hutsemékers, D., Surdej, J. 2008, The Nuclear Region, Host Galaxy and Environment of Active Galaxies, ed. Benítez E., Cruz-González I., & Krongold Y., RevMexAA (SC) Vol. 32, 83
Snedden, S. & Gaskell, C. 2004, in ASP Conf. Ser. 311, AGN Physics with the Sloan Digital Sky Survey, ed. G. T. Richards & P. B. Hall, 197
Statler, T. S. 1995, AJ, 109, 1371
Sulentic, J. W., Marziani, P., Dultzin-Hacyan, D., Calvani, M., & Moles, M. 1995, ApJ, 445, 86
Sulentic, J. W., Marziani, P., & Dultzin-Hacyan, D. 2000, ARA&A, 38, 521
Sulentic, J. W., Repetto, P., Stirpe, G. M., Marziani, P., Dultzin-Hacyan, D., Calvani, M. 2006, A&A, 456, 929
Tonry, J. & Davis, M. 1979, AJ, 84, 1511
Vanden Berk, D. E., Shen, J., Yip, C.-W., Schneider, D. P., Connolly, A. J., Burton, R. E., Jester, S., Hall, P. B., Szalay, A. S., & Brinkmann, J. 2006, AJ, 131, 84
Van Der Marel, R. & Franx, M. 1993, ApJ, 407, 525
Véron-Cetty, M.-P., Joly, M., & Véron, P. 2004, A&A, 417, 515
Véron-Cetty, M.-P. & Véron, P. 2006, A&A, 455, 773
Vestergaard, M., Wilkes, B. J., & Barthel, P. D. 2000, ApJ, 538, L103
Wandel, A. 1999, ApJ, 519, 39
Wandel, A., Peterson, B.M., & Malkan, M. A. 1999, ApJ, 526, 579
Yip, C.-W., Connolly, A. J., Szalay, A. S., Budavári, T., SubbaRao, M., Frieman, J. A., Nichol, R. C., Hopkins, A. M., York, D. G., Okamura, S. 2004a, AJ, 128, 585
Yip, C.-W., Connolly, A. J., Vanden Berk, D. E., Ma, Z., Frieman, J. A., SubbaRao, M., Szalay, A. S., Richards, G. T., Hall, P. B., Schneider, D. P. 2004b, AJ, 128, 2603